

# Evolving photonic authentication with sustainable luminescent smart e-tags

Lília M. S. Dias<sup>1,2</sup> | Lianshe Fu<sup>1</sup> | R. F. P. Pereira<sup>3</sup> | Albano N. Carneiro Neto<sup>1</sup>  | V. de Zea Bermudez<sup>4</sup> | P. S. André<sup>2</sup> | Rute A. S. Ferreira<sup>1</sup> 

<sup>1</sup>Department of Physics and CICECO—Aveiro Institute of Materials, University of Aveiro, Aveiro, Portugal

<sup>2</sup>Department of Electrical and Computer Engineering and Instituto de Telecomunicações, Instituto Superior Técnico, Universidade de Lisboa, Lisbon, Portugal

<sup>3</sup>Chemistry Center and Chemistry Department, University of Minho, Braga, Portugal

<sup>4</sup>Chemistry Department and CQ-VR, University of Trás-os-Montes e Alto Douro, Vila Real, Portugal

## Correspondence

Rute A. S. Ferreira and P. S. André.

Email: [rferreira@ua.pt](mailto:rferreira@ua.pt) and [paulo.andre@lx.it.pt](mailto:paulo.andre@lx.it.pt)

[andre@lx.it.pt](mailto:andre@lx.it.pt)

## Funding information

Fundação para a Ciência e a Tecnologia, Grant/Award Numbers: UI/BD/153491/2022, UID/EEA/50008/2021, UIDB/50011/2020, UIDP/50011/2020 & LA/P/0006/2020, UIDB/00686/2020, UIDP/00686/2020

## Abstract

Counterfeiting remains a significant threat, causing economic and safety concerns. Addressing this, authentication technologies have gained traction. With the rise of the Internet of Things, authentication is crucial. Photonic Physical Unclonable Functions (PUFs) offer unique identifiers. We present low-cost and sustainable e-tags that may be printed virtually on any surface for authentication due to the bespoke texturization of sustainable inks of surface-modified carbon dots. A single e-tag provides randomized phosphorescence (or afterglow) patterns, which provide multiple layers of safety by exploiting different patterning, excitation energies, and temporal characteristics. A comprehensive case study employing photonic challenge-response pairs, involving a sample size of up to  $2^9$  emission spectra in combination with  $10^2$  photographs taken with a smartphone, displays a low authentication probability of error ( $<10^{-11}$ ), which supports the potential of our combined approach toward the development of more robust photonic PUF systems.

## KEYWORDS

carbon dots, Internet of things, light emitting diode, physical unclonable functions

## 1 | INTRODUCTION

Counterfeit goods significantly threaten global economies, impacting world trade by about 2.5% of its value. In Europe, 5.8% of imports suffer from fake goods,<sup>1</sup>

underlining the severity of modern global economies. Evolving technology further empowers criminal networks to adapt swiftly. Yet, despite public awareness, protecting brands remains secondary. This emphasizes the urgent requirement for cost-effective, universally

This is an open access article under the terms of the [Creative Commons Attribution](https://creativecommons.org/licenses/by/4.0/) License, which permits use, distribution and reproduction in any medium, provided the original work is properly cited.

© 2024 The Authors. FlexMat published by John Wiley & Sons Australia, Ltd on behalf of Nanjing University of Posts & Telecommunications.

applicable authentication technologies to fortify anti-counterfeiting strategies.

Current anti-counterfeiting technologies such as digital prints, Quick-Response codes, near-field communication chips, non-fungible tokens, and tracking software have limitations against complex threats from the expanding Internet of Things (IoT).<sup>2</sup> The rise of digital ecosystems demands efficient, secure cryptographic key generation methods. Physical Unclonable Functions (PUFs) offer promise by using unpredictable processes to reduce duplication risks.<sup>3,4</sup> The PUF is a physical entity that generates a unique output based on its inherent physical characteristics. These characteristics are usually influenced by manufacturing variations, imperfections, or random processes during fabrication, making each instance of the PUF unique. Therefore, they are inherently difficult to replicate or clone and are more resistant to tampering as their properties are not easily modified without damaging the device. The PUFs are based on black-box challenge-response pairs (CRPs), generating unique and unpredictable responses to the external stimuli.<sup>5</sup> Photonic PUFs provide additional advantages, surpassing electronic PUF limitations in cost, sustainability, energy, and cyber-attack vulnerability.<sup>4</sup>

Early photonic PUF efforts utilized laser-based speckle patterns<sup>4</sup> and also explored random number generation.<sup>6</sup> Recent advancements leverage tunable luminescent materials, relying on emission properties such as intensity, wavelength, and lifetimes.<sup>7,8</sup> Single-level methods create microscopic or macroscopic luminescent patterns using a single excitation wavelength, detectable via hyperspectral microscopy<sup>9</sup> optical microscopy,<sup>10,11</sup> or a charge-coupled device (CCD) from a smartphone.<sup>12</sup> Multi-level PUFs include transient luminescence to produce dynamic random patterns accessed through fluorescence microscopy.<sup>13</sup>

To bolster PUF-based authentication robustness, increasing the number of CRPs by combining diverse detectable physical features proves effective. Nonetheless, the examples rely on complex detection methods, namely surface-enhanced scattering detected via confocal Raman combined with macroscale multicolor fluorescence visible on a smartphone,<sup>8</sup> light scattering recognized via smartphones, coupled with random emission intensity distributions analyzed through hyperspectral microscopy.<sup>9</sup> Also, techniques such as white-light luminescence and second harmonic generation,<sup>14</sup> or macroscale color change along with microscopic and 3D structural data analyzed through portable or high-resolution fluorescence microscopes<sup>13</sup> make multi-level anti-counterfeiting tags a challenge for widespread use. Enhancing the robustness of photonic PUFs demands new methods to generate uncorrelated responses between different PUFs under the same

challenge.<sup>12,15</sup> Some reports confirm the unpredictability and uncorrelation of keys in photonic PUFs according to certified standards.<sup>16,17</sup>

The integration of PUFs poses challenges and opportunities in communication protocols, privacy, and security. PUFs provide unique device identifiers, enhancing authentication and communication security.<sup>18</sup> They generate identifiers without personal data, yet concerns about tracking exist, addressable through encryption. PUFs offer heightened security against cloning and tampering, but vulnerabilities like replay attacks require cryptographic measures. Overall, PUF integration enhances IoT security, though protocol adjustments and privacy considerations are necessary.

We propose a method based on sustainable e-tags from carbon dots (CDs),<sup>19</sup> as a pivotal case for multi-tiered photonic PUFs. These CDs, when exposed to low-power excitation sources like LEDs or smartphone flashlights, emit detectable luminescence and patterns captured by standard CCD cameras. We studied the emission spectra from five CD-based samples, using them as PUF responses to multi-wavelength excitations achieved by combining up to 9 LEDs (2<sup>9</sup> CRPs). Additionally, we integrate the phosphorescence emission spectrum as an augmented CRP toward heightening PUF resilience. Our exploration extends to photographs of CD-based randomized luminescent patterns, amplifying e-tag authentication potential. Our methodology not only ensures cost-effectiveness but also supports effortless scalability, fortifies robustness, and enables personalized e-tag designs. Leveraging CDs' low toxicity, stability, and hydrophilicity, these tags offer versatile authentication capabilities.<sup>19</sup> This comprehensive study on photonic luminescent PUFs aimed at augmenting the CRP count, signaling progress toward sustainable smart e-tags for photon-based authentication.

## 2 | RESULTS AND DISCUSSION

### 2.1 | The e-tag concept and fabrication

The CDs-based e-tags are adaptable for printing (inkjet, spraying, spin-coating, drop cast) on diverse substrates (paper, plastic, textile), akin to printable electronic circuits. In this work, the e-tags were created by applying a suspension of CDs onto commercial non-fluorescent paper via spraying and dropping cast methods. The pattern can be adjusted by varying the suspension concentration and the processing (e.g., nozzle size). Since the PUFs response is converted into a digital key based on the spatial distributions of the emitting centers, the inherent randomness introduced by such deposition of the CDs

onto the substrate contributes significantly to the unclonability. This randomness arises from the experimental variability in the deposition methods, surface interactions, and nanoparticle properties, resulting in a unique and unpredictable physical configuration that forms the basis of the PUF robustness.

Optical features are challenged in UV and visible spectral ranges using several ( $N$ ) commercial LEDs or smartphone flashlights. Time-gated detection, revealing emission seconds post-exciting source cessation ( $t$ ), adds another layer arising from using photoluminescent CDs with phosphorescence emission. The responses are the emission spectra or the luminescent pattern images transformed into digital keys (Figure 1A), yielding  $2^N \times (t + 1)$  CRPs.

In general, CDs are intriguing nanoparticles (<10 nm) formed by a carbon-based core and tunable optical properties achieved through surface functionalization.<sup>19</sup> To cover visible emission colors, we selected six organic molecules, yielding distinct CD families with visible phosphorescence. These samples comprise spherical nanoparticles with sizes ranging from  $2.2 \pm 0.5$  to  $5 \pm 1$  nm, as shown in transmission electron microscopy (TEM) images (Figure 1B–M). High-resolution TEM images reveal a highly crystalline structure analogous to graphene,<sup>20–22</sup> and an interplanar spacing of  $\sim 0.18$  nm (Figure S1), which is consistent with the (103) diffraction plane of graphitic carbon.<sup>23,24</sup> XPS analysis indicates feature peaks for C1s, O1s, and B1s, with O and B dominating the surface composition (Figures S2–S6), while Raman spectra suggest the presence of alkali borate glasses,<sup>25</sup> particularly vitreous  $B_2O_3$  (Figures S7–S9, Scheme S2), which is further supported by the XRD patterns (Figure S10).

## 2.2 | Photoluminescence properties

The emission spectra (Figure 2A) display broad bands across the visible spectral region, with intensity varying based on excitation energy (Figure 2B). The emission color is perceptible to the naked eye under LED or flashlight illumination (Figure 2C) and ranges from blue (0.18, 0.20) to yellow (0.47, 0.44), covering bluish-green (0.20, 0.36), yellow-green (0.43, 0.53), and yellowish-green (0.30, 0.53) regions (Figure 2D). Such tunable emission results from the surface modification of the CD,<sup>26</sup> providing multiple excitation energies as the excitation spectra point out (Figure 2B). When the excitation is turned off, a delayed emission is observed (Figure 2C), as detailed below. Additionally, high absolute emission quantum yields, up to 0.52, ensure the

emission activation using easily accessible low-power sources, highlighting the potential of the selected CDs for practical usefulness across various lighting situations.

## 2.3 | Multiple challenge-response pairs

Our proposal involves generating photonic PUFs through multi-excitation wavelength combinations and phosphorescence time gating. As a proof of concept, we tested 8 or 9 LEDs, resulting in  $2^8$  (Figure 3A,B) or  $2^9$  (Figure 3C) distinct spectra, respectively. These stem from the  $C_j^i$  excitation combinations, where  $i$  signifies the number of represented LEDs and  $j$  represents their combination (Tables S1–S3). The spectra show inherent CD emissions overlapping with LEDs' emissions. For clarity, Figure 3E–G displays 10 distinct multi-wavelength excitations for CD1, CD2, and CD3, respectively.

Taking advantage of the long-lived emission, we introduced time-gating as an additional challenge to illustrate time-gated photonic PUFs. Although all the samples exhibit time-dependent emission (Figures S11–S14), we selected the mixed sample CD4 (composed of CD4-A and CD4-B) due to its higher absolute emission quantum yield (0.52) and potential to explore emission component overlaps characterized by different timescales. Figure 4 demonstrates spectral changes after the excitation is turned off. The CD4-A emission spectra show a long-lived component at 510 nm (Figure 4B) and a shorter-lived blue emission ( $\sim 440$  nm) with a lifetime value of around  $0.56 \pm 0.06$  s. The CD4-B spectra reveal variations in the relative intensity for  $\sim 475$  and  $\sim 550$  nm (Figure 4C) components with longer lifetime values ( $0.62 \pm 0.01$  and  $0.65 \pm 0.01$  s, respectively). The prolonged emission has been attributed to the  $B_2O_3$  host due to (i) the introduction of an electron-withdrawing B atom with vacant p orbitals reduces the energy of the singlet excited state, facilitating intersystem crossing and increasing triplet excitons; and (ii) covalent B–C bonds between CDs, structural rigidity, and spatial confinement within the  $B_2O_3$  polycrystalline network restrict nonradiative transitions, isolating quenchers from the environment and preserving the CDs' phosphorescence.<sup>27</sup> The mixed sample (CD4) benefits from these distinct time-dependent effects, displaying a narrower, time-dependent broadband centered around 510 nm post-exciting source cessation (Figure 4D). The formation of the CD4 sample via a physical mixture of 80% CD4-A and 20% CD4-B has led to the investigation of energy transfer (ET) between these distinct CD components, mainly concerning ET between phosphorescence bands (triplet, T) of CD4-B (donor) and CD4-A (acceptor). The emission bands of CD4-A and CD4-B are in the same

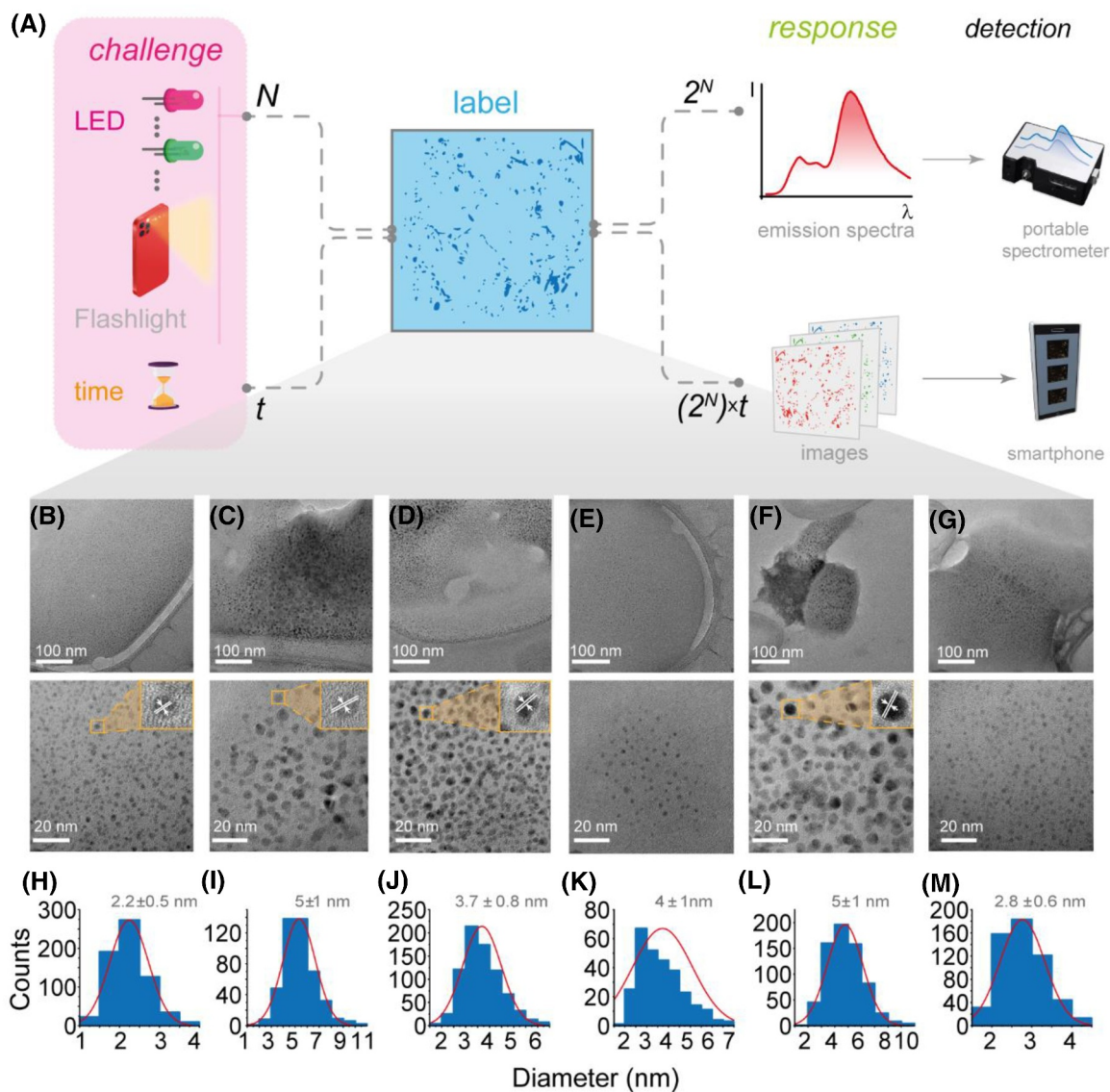


**FIGURE 1** Sustainable smart e-tags for photonic authentication. (A) The tags are printed in a flexible personalized design and size. A number of challenges ( $2^N + 1$ ) can be achieved either by tuning the wavelength of the commercial LEDs or by using the flashlight of a smartphone and the responses are based on the emission spectra or images of luminescent random patterns acquired when the excitation is turned on and off. (B–G) TEM images and (H–M) the size distribution of CD1, CD2, CD3, CD4-A, CD4-B, and CD5, respectively; insets reproduce the HR-TEM images of individual CDs showing lattice fringes with the corresponding d-spacing ( $\sim 0.2$  nm) determined by Fast Fourier Transform (FFT) analysis.

spectral range, providing a resonant spectral overlap (Figure S17).<sup>28</sup> Moreover, the band profile of the phosphorescence spectra of the mixed compound (CD4) shows a relative intensity decrease of the two main peaks ascribed to CD4-B, while CD4-A remains unchanged (Figure S18 and Figure 4). In addition, the full width at half maximum of the phosphorescence band of the mixed sample CD4 ( $3700\text{ cm}^{-1}$ ) is larger than that of CD4-A ( $2580\text{ cm}^{-1}$ ) and smaller than that of CD4-B ( $4670\text{ cm}^{-1}$ ) (Figure S19), further supporting that CD4-B acts as the ET donor and CD4-A acts as the acceptor.

The evaluation of the PUFs' performance was focused on using excitation and emission spectra as CRPs. Emission spectra underwent analysis via Power Spectral Density and bit-key transformation (Supporting Information S5.1)<sup>16</sup> for Hamming Distance (HD) comparison (Equation S3, Supporting Information S5.3). Each excitation is considered a unique challenge. Different excitations were anticipated to yield non-repeated spectra (Inter-HDs), while repetitions of the same excitation were anticipated to generate similar responses (Intra-HDs). HD values were represented in

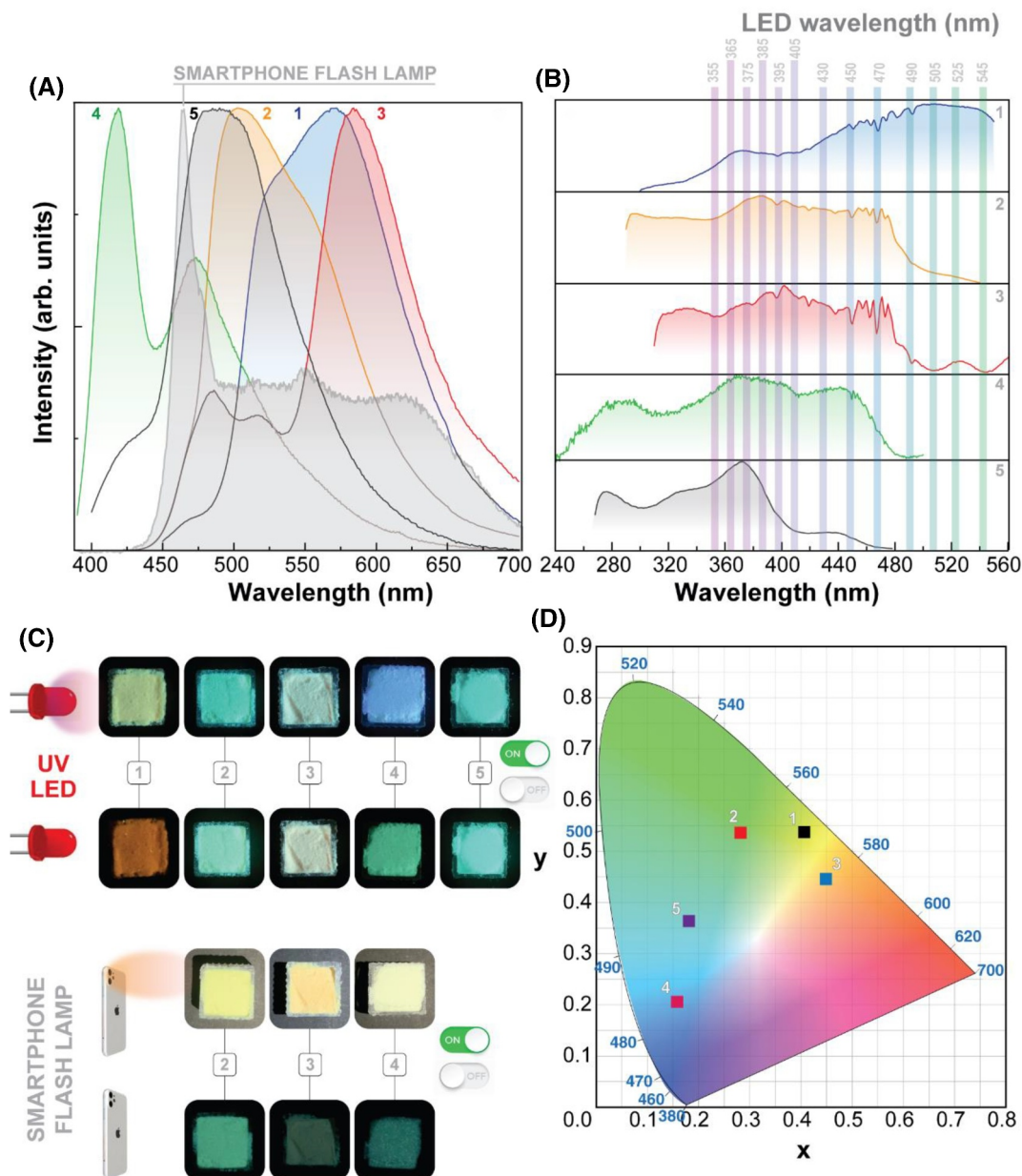


**FIGURE 2** Photoluminescence features and color coordinates. (A) Emission spectra excited at 430 nm (CD1), 400 nm (CD2, CD3), 370 nm (CD4), and 380 nm (CD5); the gray shadow is the flash lamp emission spectrum. (B) Excitation spectra monitored at 570 nm (CD1), 555 nm (CD2), 585 nm (CD3), 520 nm (CD4), and 495 nm (CD5). (C) Photographs ( $1 \times 1 \text{ cm}^2$ ) under UV or smartphone flash lamp. (D) CIE chromaticity diagram.

histograms, fitted to Gaussian probability density functions (*pdfs*), and weighted based on occurrence probabilities (Figure S15). Optimal separation values were identified, resulting in low error probabilities for CD1 (0.03), CD2 (0.05), and CD3 (0.01), whereas CD4 (0.27) and CD5 (0.17) exhibited higher error probabilities due to their optical properties impacting the similarity of emission properties. CD3 demonstrated superior authentication performance and key

characteristics (Table S4). The addition of CD4 phosphorescence emission as a response (Figure S15 and S16) impacted the error probability, decreasing from 0.27 to 0.08, elevating authentication accuracy and precision. This underlined the afterglow's potential as an additional challenge, enhancing authentication robustness without hindering key reproducibility. Authentication performance and key characterization metrics for CD1–5 are detailed in Table S4. To enhance

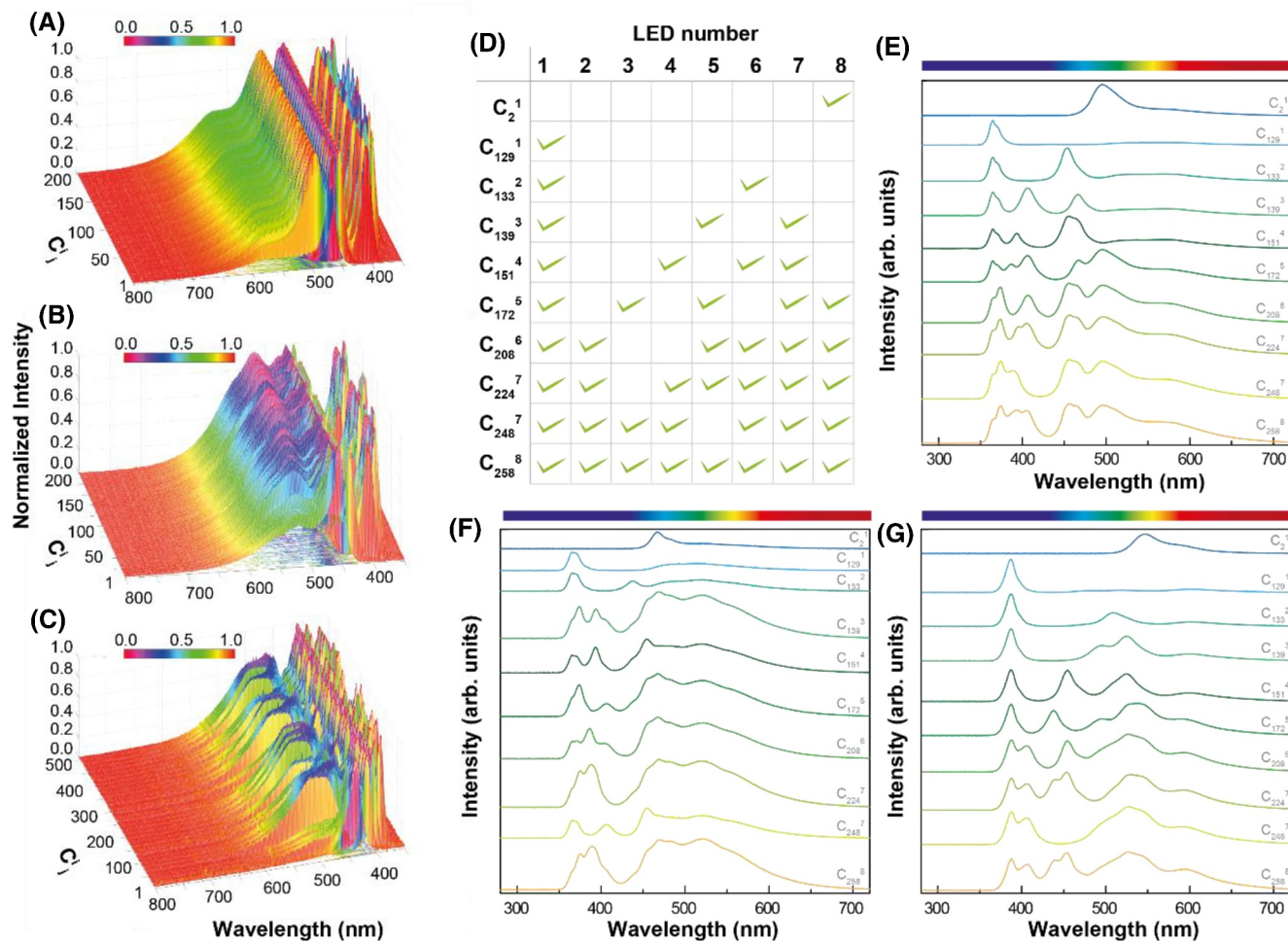


FIGURE 3 Multi-excitation photonic PUFs. Emission spectra excited under 8 (or 9) different LEDs for (A) CD1, (B) CD2, and (C) CD5. (D) selected  $C_j^i$  conditions for (E) CD1, (F) CD2, and (G) CD3.

the error probability values, we propose combining the CD emission features with their ability to be processed as randomized luminescent patterns, on which it is possible to employ an image-based authentication.

## 2.4 | Mobile smart e-tags

As the CDs are nano-sized particles (Figure 1), their deposition as coatings providing a random distribution of the emitting centers, so that distinct CRPs are attained. Figure 5 illustrates the photos (responses) of selected e-tags, that were converted to binary keys (Equations S1 and S2), and compared with each other. The HD values were represented in histograms and fitted to Gaussian *pdfs*, one centered at a lower value (intra-HDs, between responses from the same PUF under repeated challenges) and a higher value (inter-HDs, between responses from different PUFs under the

same challenge or responses from the same PUF under different challenges). Similarly to the previous analysis, the *pdfs* were weighted according to the probability of occurrence of each prediction.

Employing the same challenge (excitation wavelength 365 nm) in distinct e-tags (Figure 5A), the HD values (Figure 5D) distinguish images from the same tag (blue zones) and between different tags (orange zones). The achieved optimal separation value of HD ( $d_{opt}$ ) is 0.18 with a probability of error of  $7.2 \times 10^{-11}$  (Figure 5E). A similar study was performed for an e-tag under different challenges (excitation wavelengths 365 nm, 385 nm, 405 nm, and smartphone flash, Figure 5B), where a probability of error of  $3.3 \times 10^{-4}$  for  $d_{opt} = 0.10$  was attained (Figure 5F,G). For both approaches, the accuracy, precision, and recall values (Equation S8 and S10) are greater than 99.99%, 99.94%, and 99.94%, respectively. In addition, the keys were characterized in terms of uniformity, uniqueness,

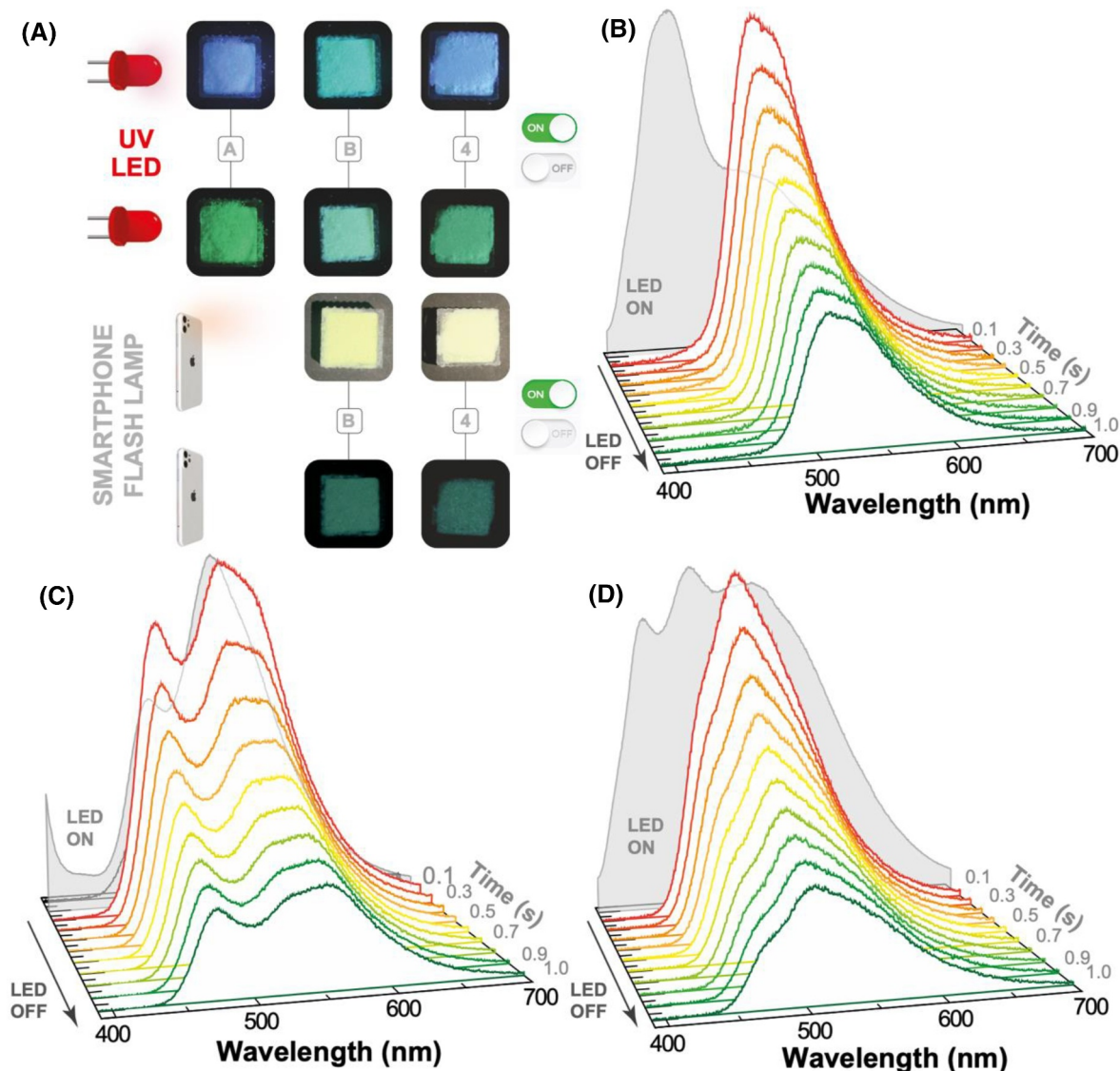


**FIGURE 4** Time-dependent optical features. (A) Photographs taken using a UV source and the flashlight from a smartphone. Emission spectra of (B) CD4-A, (C) CD4-B, and (D) CD4, when the excitation (365 nm) is turned on and after the excitation has been turned off.

reliability, and mean bit aliasing (Equations S4–S7), revealing figures of 50%, 48%, 97%, and 50% (Figure 6A) and 50%, 37%, 97%, and 50% (Figure 5B) that indicate high reproducibility.

The e-tags were also challenged by time, as illustrated in Figure 5C under LED excitation acquired at two distinct instants (Figure 5c1,c2) and after the excitation has been turned off (Figure 5c3–c32). The difference between one image of the tag under LED excitation (response 1) and those of the phosphorescence (response 2–32) yields an HD around 0.2 that increases as the challenged time increases (Figure 5H,I).

The methodologies presented here stand out due to the e-tag sustainability and easy processing, combined with simple and ubiquitous detection (Table S5).

### 3 | CONCLUSIONS

In this work, single e-tags based on phosphorescent CDs were developed and demonstrated potential for enhanced photonic PUFs by exploiting emission spectra-based responses alongside photos of randomized luminescent patterns. The developed e-tags underscore the potential of sustainable luminescent materials in developing more resilient photonic PUF systems, capable of offering multi-level detectable responses. Although the integration of PUFs with IoT introduces challenges such as the necessity for protocol adjustments and concerns regarding privacy, their distinctive attributes present significant opportunities for enhancing security and mitigating threats across the IoT landscape.

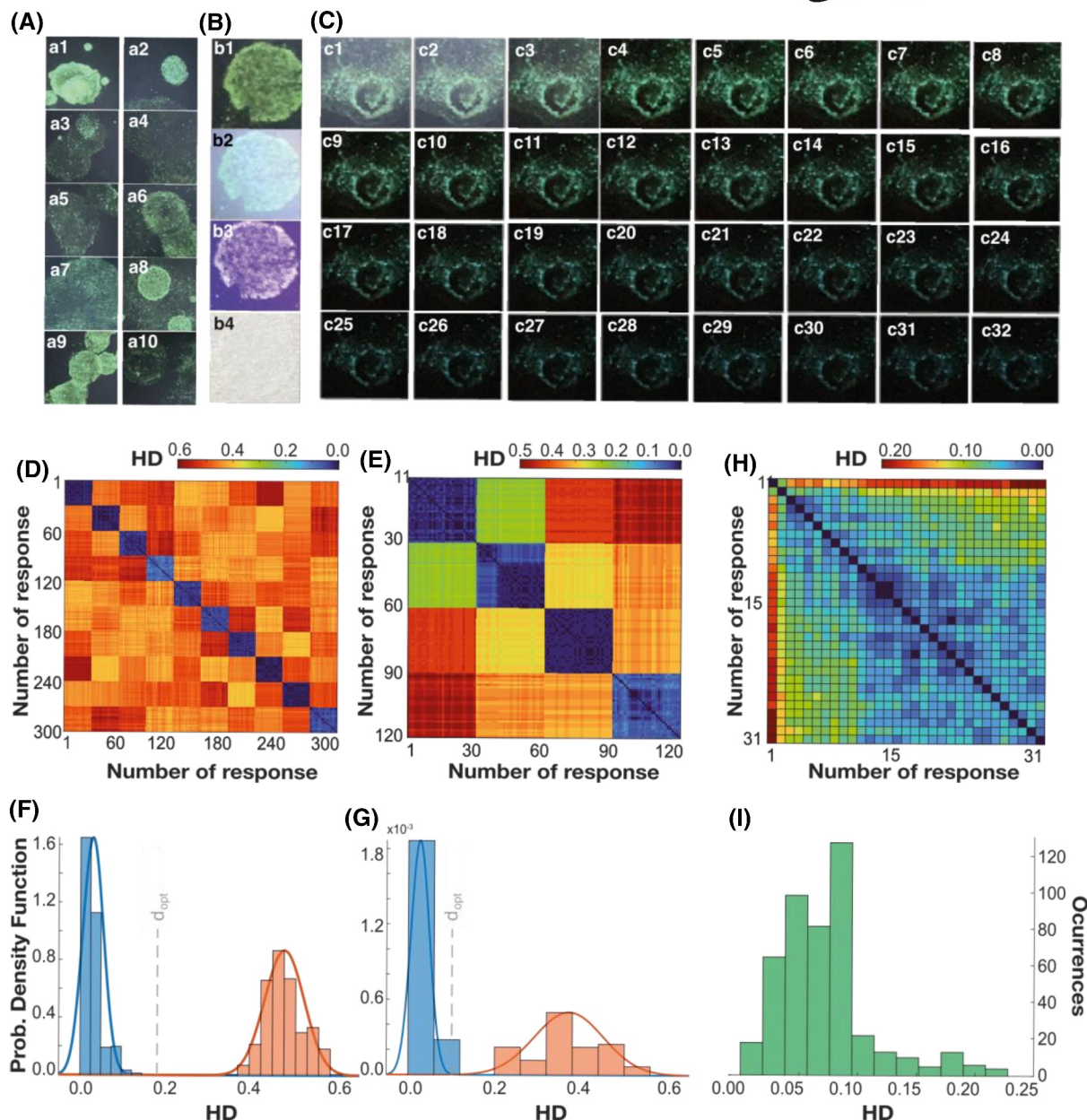


**FIGURE 5** Selected e-tags based on photonic PUFs. Photographs of (A) 10 distinct e-tags based on CD2 excited at 365 nm; (B) a single e-tag based on CD2 excited at 365 nm (b1), 385 nm (b2), 405 nm (b3), and smartphone flash (b4); (C) single e-tag based on a mixed CDs tag excited at 365 nm (c1, c2) and after the excitation is turned off (c3–c32) acquired with a time step of 0.17 s. (D, F, H) Hamming distances and normalized histograms of (E, G) the probability density and the optimum decision value ( $d_{opt}$ ) and (I) occurrences for case studies (A), (B), and (C), respectively.

## 4 | EXPERIMENTAL SECTION/METHODS

### 4.1 | Materials

Sodium cholate hydrate (SC), fluorescein (FL), coumarin-3-carboxylic acid (CCA), naphthalene-2,6-dicarboxylic acid (NDCA), rhodamine B (RhB), dibenzoylmethane (DBM), boric acid (BA) (Scheme S1), and ethanol (EtOH) were used as received. Five CDs with phosphorescence

emission were synthesized, and designated as CD1, CD2, CD3, CD4, and CD5. To provide tunable emission covering the visible spectral range, distinct synthesis strategies were followed.

**CD1.** 0.5 mg of SC (0.05 mL SC in EtOH, 10.0 mg/mL) was mixed well with 0.5 g of BA. The mixture was calcinated at 230°C for 7 min, taken out from the oven, and cooled down to room temperature. **CD2.** 0.5 mg of FL (0.25 mL of FL in EtOH, 2.0 mg/mL) and 1.5 mg of CCA (0.75 mL of CCA in EtOH, 2.0 mg/mL) were mixed

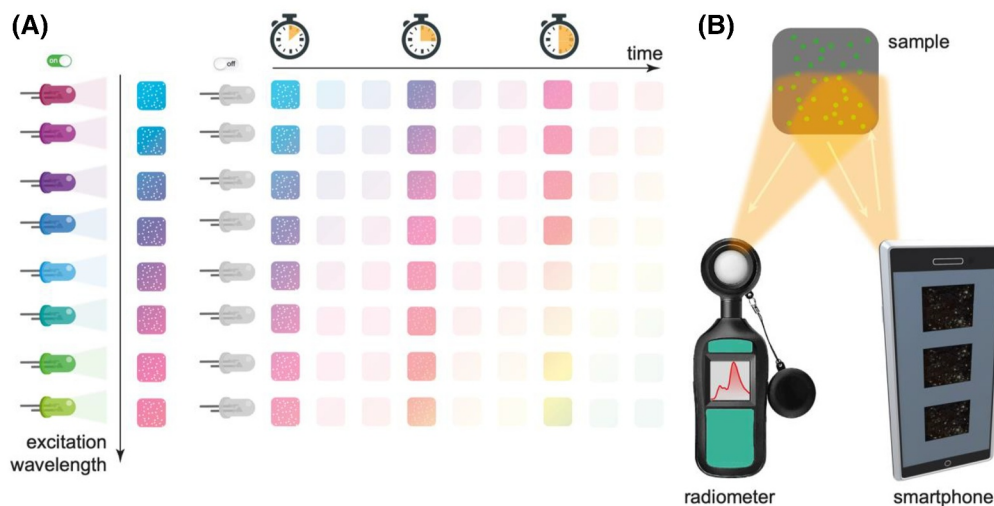


**FIGURE 6** Schematic representation of the proposed PUF, with (A) the proposed challenges (excitation wavelength and time after the excitation is turned off) and (B) the respective responses acquired by a smartphone.

well with 1.0 g of BA. The mixture was calcinated at 230°C for 9 min, taken out from the oven, and cooled down to room temperature. **CD3.** 0.5 mg of FL (0.25 mL of FL in EtOH, 2.0 mg/mL), 1.0 mg of NDCA (0.5 mL of NDCA in EtOH, 2.0 mg/mL), and 0.05 mg RhB (0.021 mL of RhB in EtOH, 2.4 mg/mL) were mixed well with 1.0 g of BA. The mixture was calcinated at 230°C for 9 min, taken out from the oven, and cooled down to room temperature. **CD4.** It is a mixture of **CD4-A** and **CD4-B**. For synthesis of **CD4-A**: 10.0 mg of DBM (0.40 mL of DBM in EtOH, 25.0 mg/mL) was mixed well with 1.0 g of BA. The mixture was calcinated at 225°C for 15 min, taken out from the oven, and cooled down to room temperature. For synthesis of **CD4-B**: 96 mg of RhB was dissolved in 15 mL of a 0.67 M NaOH solution with ultrasonic treatment. Then, the clear solution was transferred into a poly(tetrafluoroethylene)-lined autoclave (20 mL) and heated at 180°C for 8 h and cooled down to room temperature naturally. The resulting aqueous solution was diluted to 20 mL with water and named as RhBCDs. 0.25 mL of RhBCDs aqueous solution was mixed with 2.0 g BA. The solid was ground and dried at 90°C to get a dried powder. The powder was calcinated at 235°C for 15 min, moved out of the oven, and cooled down to room temperature naturally. **CD4** was obtained by mixing **CD4-A** and **CD4-B** in a weight ratio of (4:1). The mixture was ground, and then the pellet was made for measurements. **CD5.** 1.5 mg of CCA (0.3 mL CCA in EtOH, 5.0 mg/mL) was mixed well with 0.5 g of BA. The mixture was calcinated at 230°C for 10 min, taken out from the oven, and cooled down to room temperature. The protection role from the matrix boron oxide ensures the afterglow property and stability under normal atmospheric conditions.

## 4.2 | Unclonable tag based on luminescent random patterns

The CDs were processed as unclonable tags, by being grounded and dispersed in n-hexane and dropped on a commercial non-fluorescent paper. CD2 and CD-mixed (CD1, CD2, CD3, and CD5 with a weight ratio 1:1:1:1) were selected. The solvent was evaporated at room temperature.

## 4.3 | Characterization techniques

TEM images were obtained at the Iberian Nanotechnology Laboratory using a JEOL JEM 2100 (200 kV) microscope. Samples were dispersed in water and placed into the analyzing grids (UC-A on holey 400 mesh Cu grids, Ted Pella ref. 01824) by drop-casting, followed by drying at room temperature. XPS was performed by an ESCALAB 25Xi (Thermo Fisher Scientific) using a monochromated Al K $\alpha$  ( $h\nu = 1486.68$  eV) radiation, operated at 220 W, 14.6 kV, and a spot size of 650  $\mu\text{m}$ . XPS spectra were collected at pass energies of 100 and 40 eV, for survey spectra and individual elements, respectively. The energy step for individual elements was 0.1 eV. XPS spectra were peak-fitted using Avantage data processing software (Thermo Fisher Scientific) and the Shirley-type background was used. All the XPS peaks were referenced to adventitious carbon C1s, C–C peak at 284.8 eV. Quantification was done using sensitivity factors provided by the Avantage library. Charge neutralization was achieved with both low energy electron and argon ion Flood guns (<0.1 eV, 120 and 70  $\mu\text{A}$  current, respectively).

#### 4.4 | Optical studies

The photoluminescence spectra were recorded with a modular double-grating excitation spectrofluorimeter with a TRIAX 320 emission monochromator (Fluorolog-3, Horiba Scientific) coupled to an R928 Hamamatsu photomultiplier. The spectra were corrected for the detection and optical spectral response of the spectrofluorimeter. The emission quantum yield values were measured at room temperature using a system (C9920-02, Hamamatsu) with a 150 W xenon lamp coupled to a monochromator for wavelength discrimination, an integrating sphere as the sample chamber, and a multi-channel analyzer for signal detection. The method is accurate to within 10%.

#### 4.5 | Optical features and image acquisition

The emission spectra under continuous excitation of different wavelengths were obtained using several LEDs emitting at distinct wavelengths (Tables S1–S3), as detailed in the Supporting Information. Figure 6 is a schematic representation of the proposed PUF with the different challenges (excitation wavelength and afterglow time) and the possible methods to acquire the responses, the emission spectrum with a spectrometer, and the image-based response with a common smartphone.

#### AUTHOR CONTRIBUTIONS

Rute A. S. Ferreira and P. S. André directed and designed the project. Lianshe Fu performed the sample preparation, and V. de Zea Bermudez and R. F. P. Pereira characterized the samples by TEM, XPS, Raman spectroscopy and XRD; Albano N. Carneiro Neto studied the energy transfer features and spectral analysis, Lília M. S. Dias performed the optical characterization. Rute A. S. Ferreira and P. S. André supervised the whole project. All the authors contributed to the manuscript writing.

#### ACKNOWLEDGMENTS

This work was developed within the scope of the project CICECO-Aveiro Institute of Materials, UIDB/50011/2020, UIDP/50011/2020 & LA/P/0006/2020, financed by national funds through the FCT/MCTES (PIDDAC) and Instituto de Telecomunicações (UID/EEA/50008/2021). LMSD thanks FCT for a PhD grant (UI/BD/153491/2022). SFH Correia (IT) and JFCB Ramalho (CICECO) are acknowledged for support in the emission data acquisition and JP Seifert and N. Wisiol (Technische Universität Berlin) for fruitful discussion about strong PUFs. RFPP acknowledges FCT for CQUM base and programmatic

projects (UIDB/00686/2020 and UIDP/00686/2020) and FCT-UMinho for the contract in the scope of Decreto-Lei 57/2016 (DL 57/2016/CP1377/CT0050, DOI: 10.54499/DL57/2016/CP1377/CT0050).

#### CONFLICT OF INTEREST STATEMENT

Rute A.S. Ferreira is an editorial board member of this journal and was not involved in the editorial review or the decision to publish this article. The authors declare no conflict of interests.

#### DATA AVAILABILITY STATEMENT

The authors declare that all data supporting the findings of this study are available within the paper and Supplementary Information. Other supporting data are available from the corresponding author upon request.

#### ORCID

Albano N. Carneiro Neto  <https://orcid.org/0000-0003-2432-0992>

Rute A. S. Ferreira  <https://orcid.org/0000-0003-1085-7836>

#### REFERENCES

1. *Global Trade in Fakes: A Worrying Threat*, in *Illicit Trade*, OECD Publishing, Paris **2021**.
2. J. F. C. B. Ramalho, S. F. H. Correia, L. Fu, L. M. S. Dias, P. Adão, P. Mateus, R. A. S. Ferreira, P. S. André, *npj Flex Electron* **2020**, *4*, 11.
3. C. Mesaritis, M. Akriotou, A. Kapsalis, E. Grivas, C. Chaintoutis, T. Nikas, D. Syvridis, *Sci Rep* **2018**, *8*, 9653.
4. R. Pappu, B. Recht, J. Taylor, N. Gershenfeld, *Science* **2002**, *297*, 2026.
5. B. T. Bosworth, I. A. Atakhodjaev, M. R. Kossey, B. C. Grubel, D. S. Vresilovic, J. R. Stroud, N. MacFarlane, J. Villalba, N. Dehak, A. B. Cooper, M. A. Foster, A. C. Foster, *APL Photonics* **2020**, *5*, 010803.
6. L. M. S. Dias, T. F. S. Silvério, R. A. Sá Ferreira, P. S. de Brito André, *IET Optoelectron* **2022**, *16*, 174.
7. S. Liu, L. Yan, Q. Li, J. Huang, L. Tao, B. Zhou, *Chem Eng J* **2020**, *397*, 125451.
8. J. Wang, Q. Zhang, R. Chen, J. Li, J. Wang, G. Hu, M. Cui, X. Jiang, B. Song, Y. He, *Nano Today* **2021**, *41*, 101324.
9. T. Silvério, L. M. S. Dias, J. F. C. B. Ramalho, S. F. H. Correia, L. Fu, R. A. S. Ferreira, P. S. André, *AIP Adv* **2022**, *12*, 085316.
10. Y. Liu, F. Han, F. Li, Y. Zhao, M. Chen, Z. Xu, X. Zheng, H. Hu, J. Yao, T. Guo, W. Lin, Y. Zheng, B. You, P. Liu, Y. Li, L. Qian, *Nat Commun* **2019**, *10*, 2409.
11. J. Yang, M. Feng, J. Wang, Z. Zhao, R. Xu, Z. Chen, K. Zhang, A. Khan, Y. Han, F. Song, W. Huang, *Adv Mater* **2023**, *35*, 2306003.
12. L. M. S. Dias, J. F. C. B. Ramalho, T. Silvério, L. Fu, R. A. S. Ferreira, P. S. André, *IEEE Access* **2022**, *10*, 24433.
13. H. Chen, H. Hu, B. Sun, H. H. Zhao, Y. Qie, Z. Luo, Y. Pan, W. Chen, L. Lin, K. Yang, T. Guo, F. Li, *ACS Appl Mater Interfaces* **2023**, *15*, 2104.
14. E. Ponkratova, E. Ageev, P. Trifonov, P. Kustov, M. Sandomirskii, M. Zhukov, A. Larin, I. Mukhin, T. Belmonte, A.

- Nominé, S. Bruyère, D. Zuev, *Adv Funct Mater* **2022**, *32*, 2205859.
15. M. Akriotou, A. Fragkos, D. Syvridis, in *Physics and Simulation of Optoelectronic Devices XXVIII* (Eds: M. Osiński, Y. Arakawa, B. Witzigmann), Vol. 20, SPIE **2020**.
  16. A. Di Falco, V. Mazzone, A. Cruz, A. Fratalocchi, *Nat Commun* **2019**, *10*, 5827.
  17. A. Fratalocchi, A. Fleming, C. Conti, A. Di Falco, *Nanophotonics* **2020**, *10*, 457.
  18. A. Al-Meer, S. Al-Kuwari, *ACM Comput Surv* **2023**, *55*, 314.
  19. L. Đorđević, F. Arcudi, M. Cacioppo, M. Prato, *Nat Nanotechnol* **2022**, *17*, 112.130.
  20. L. Wang, Y. Wang, T. Xu, H. Liao, C. Yao, Y. Liu, Z. Li, Z. Chen, D. Pan, L. Sun, M. Wu, *Nat Commun* **2014**, *5*, 5357.
  21. F. Yuan, T. Yuan, L. Sui, Z. Wang, Z. Xi, Y. Li, X. Li, L. Fan, Z. Tan, A. Chen, M. Jin, S. Yang, *Nat Commun* **2018**, *9*, 2249.
  22. Y. Ding, X. Wang, M. Tang, H. Qiu, *Adv Sci* **2022**, *9*, 2103833.
  23. J. Fayos, *J Solid State Chem* **1999**, *148*, 278.
  24. S. F. H. Correia, L. Fu, L. M. S. Dias, R. F. P. Pereira, V. de Zea Bermudez, P. S. André, R. A. S. Ferreira, *Nanoscale Adv* **2023**, *5*, 3428.
  25. B. N. Meera, J. Ramakrishna, *J Non-Cryst Solids* **1993**, *159*, 1.
  26. Q. Feng, Z. Xie, M. Zheng, *Chem Eng J* **2021**, *420*, 127647.
  27. W. Li, W. Zhou, Z. Zhou, H. Zhang, X. Zhang, J. Zhuang, Y. Liu, B. Lei, C. Hu, *Angew Chem* **2019**, *131*, 7356.
  28. B. S. D. Onishi, A. N. Carneiro Neto, R. Bortoletto-Santos, V. R. Mastelaro, L. D. Carlos, R. A. S. Ferreira, S. J. L. Ribeiro, *Nanoscale* **2024**, *16*, 6286.

## SUPPORTING INFORMATION

Additional supporting information can be found online in the Supporting Information section at the end of this article.

**How to cite this article:** L. M. S. Dias, L. Fu, R. F. P. Pereira, A. N. Carneiro Neto, V. d. Z. Bermudez, P. S. André, R. A. S. Ferreira, *FlexMat* **2024**, *1*, 116.  
<https://doi.org/10.1002/flm2.16>